JACS
JOURNAL OF THE AMERICAN CHEMICAL SOCIETY

Article

pubs.acs.org/JACS

Dynamics of Energy Transfer in a Conjugated Dendrimer Driven by Ultrafast Localization of Excitations

Johan F. Galindo,[§,∥] Evrim Atas,[§,⊥] Aysun Altan,[#] Daniel G. Kuroda,[▽] Sebastian Fernandez-Alberti,[†] Sergei Tretiak,[‡] Adrian E. Roitberg,*[,§] and Valeria D. Kleiman*[,§]

[†]Universidad Nacional de Quilmes, Roque Saenz Peña 352, B1876BXD Bernal, Argentina

[‡]Theoretical Division, Center for Nonlinear Studies (CNLS) and Center for integrated Nanotechnologies (CINT), Los Alamos National Laboratory, Los Alamos, New Mexico 87545, United States

[§]Department of Chemistry, University of Florida, Gainesville, Florida 32611, United States

Supporting Information

ABSTRACT: Solar energy conversion starts with the harvest of light, and its efficacy depends on the spatial transfer of the light energy to where it can be transduced into other forms of energy. Harnessing solar power as a clean energy source requires the continuous development of new synthetic materials that can harvest photon energy and transport it without significant losses. With chemically-controlled branched architectures, dendrimers are ideally suited for these initial steps, since they consist of arrays of chromophores with relative positioning and orientations to create energy gradients and to spatially focus excitation energies. The spatial localization of the energy delimits its efficacy and has been a point of intense research for synthetic light harvesters. We present the results of a combined theoretical experimental study elucidating ultrafast, unidirectional, electronic energy transfer on a complex molecule designed to spatially focus the initial excitation onto an energy sink. The study explores the complex interplay between atomic motions, excited-state populations, and localization/delocalization of excitations. Our findings show that the electronic energy-transfer mechanism involves the ultrafast collapse of the photoexcited wave function due to nonadiabatic electronic transitions. The localization of the wave function is driven by the efficient coupling to high-frequency vibrational modes leading to ultrafast excited-state dynamics and unidirectional efficient energy funneling. This work provides a long-awaited consistent experiment−theoretical description of excited-state dynamics in organic conjugated dendrimers with atomistic resolution, a phenomenon expected to universally appear in a variety of synthetic conjugated materials.

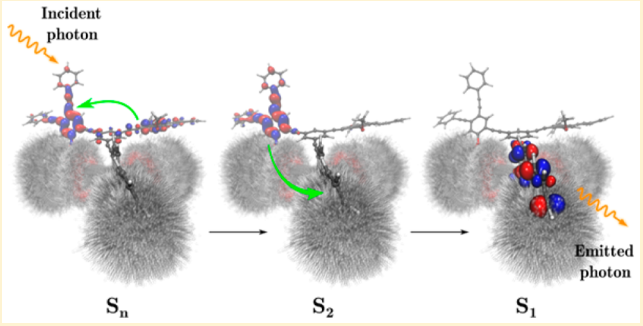

INTRODUCTION

In the quest for efficient ways to mimic natural photosynthesis, attention has been focused on the understanding of light-harvesting materials and the mechanisms for energy funneling.[1−7] The transformation of photon energy into other usable forms of energy can be helped with materials that can undergo absorption of photons by multiple chromophores, provide energy transport in the form of electronic excitation/exciton, and spatially focus that electronic energy into a target molecular system, where it can be transduced into other forms of utilizable energy. Nature itself provides numerous examples of how organisms evolved the ability of converting light into chemical energy through the use of conjugated chromophores.[7−12]

The availability of synthetic materials, like arrays of chromophores,[13] supramolecular constructs,[14] modified metal organic frameworks,[15,16] and dendrimers,[9,17−24] opens the doors to applications as organic photovoltaics, biosensors, light-emitting diodes, and other solar energy conversion applications.[25,26] In these synthetic materials, molecular architecture plays a fundamental role on the mechanism of electronic energy transfer. Understanding the interplay between architectures, dynamics, and energy transfer can lead to the development of new materials designed for higher efficiency, better photostability, and lower cost.

Light-harvesting dendritic macromolecules are branched π-conjugated systems composed of arrays of weakly coupled chromophores that absorb light at different wavelengths depending on the dendrimer's backbone structure and conformation.[27−34] Their architecture, which imposes built-in energy gradients, is responsible for their light-harvesting properties and highly efficient intramolecular energy funneling mechanism.[27,35−39]

A variety of structures have been proposed where different chromophore units are covalently attached throughout the

Received: April 20, 2015
Published: June 30, 2015

DOI: 10.1021/jacs.5b04075
J. Am. Chem. Soc. 2015, 137, 11637−11644

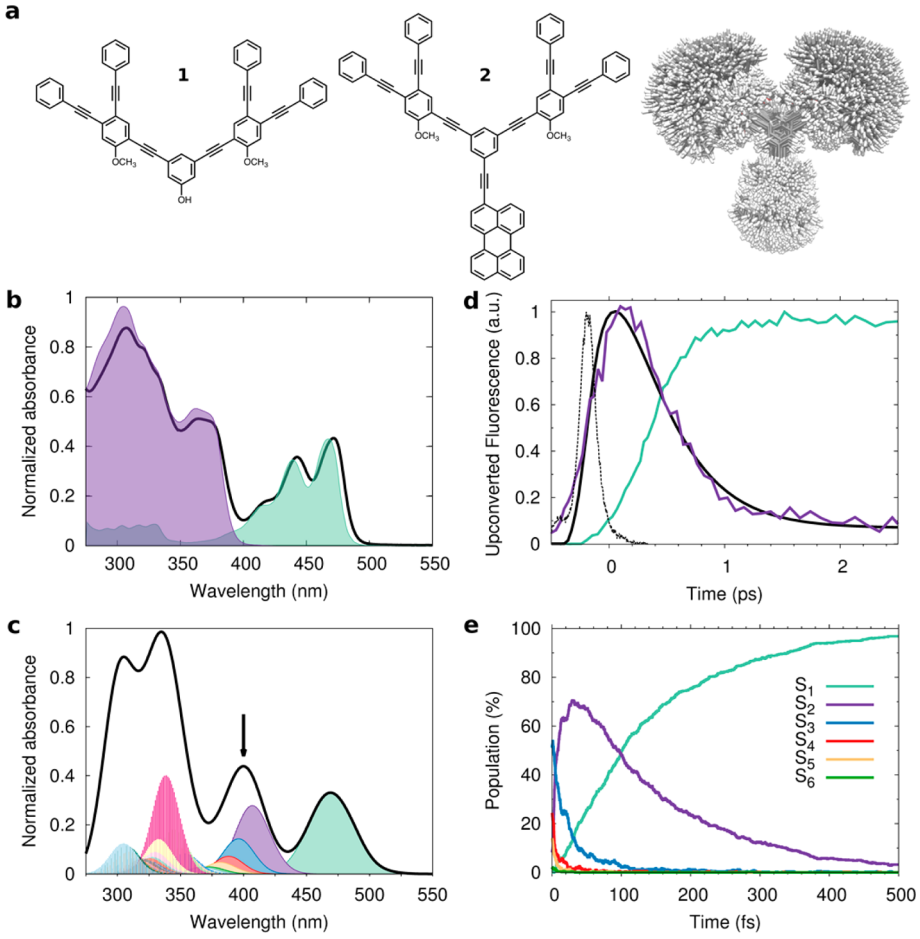

Figure 1. (a) Structures of (**1**) the model dendrimer compound, (**2**) the dendrimer with an added ethynylene-perylene as energy sink, and the 1000 different conformations of **2** obtained from QM/MM dynamics surface exploration. (b) Experimental absorption spectrum of backbone **1** (purple) energy sink EPer (green) and donor/acceptor dendrimer 2 (black) showing the lack of strong interactions between donor 1 and acceptor EPer moieties in the ground state. (c) Theoretical average spectrum of 1000 different conformations and its decomposition based on the state contributions to each excited state. The calculated spectrum agrees qualitatively with the experimental. The Franck−Condon vibrational progression of the $S_1(B1u) \leftarrow S_0(Ag)$[84] transition for ethynylene-perylene (400−500 nm) is not explicitly computed in the simulated spectrum. (d) Experimental time-resolved emission, instrument response function (dash) and simulation of the fluorescence signal with fix time constants (black); detection at 480 nm (green) probes the final sink, while detection at 400 nm(purple) probes an intermediate state. (e) Population in each excited state calculated from the number of trajectories in a state at a given time after excitation at 400 nm. Rise and decay of the populations follow the same mechanism as measured in the time-resolved emission experiments.

dendritic backbone.[28,40−43] In this work, using experiment and theoretical calculations, we elucidate the energy funneling mechanism taking place after photoexcitation of the unsymmetrical dendrimer **2** (Figure 1a). In this molecule the phenylene-ethynylene (PE) units are connected via ortho, meta, and para links, creating the required intramolecular energy gradient to achieve energy funneling to the sink (ethynylene-perylene: EPer).[27,28,44−47] Experimentally, the energy-transfer process is found to be very efficient and fast (femtoseconds time scale),[27,28,35,47−49] presenting an excellent case study of energy harvesting via a diverse and complex excited-state manifold, controlled by conformations. This system is representative of the broad class of organic semiconductor materials.[7−12] In this manuscript we present the detailed experimental and theoretical discovery of the key footprints determining the energy-transfer scenario, which involves complex dynamics of delocalized and localized excited states as well as specific vibronic coupling.

Previous reports[37,50−55] have shown the influence between nuclear dynamics and localization/delocalization of excited states in dimers where the role of nonadiabatic couplings of vibrational and electronic levels has been pointed out. It is therefore important to identify the role that nuclear differential motions in the different excited-state potential energy surfaces play on the unidirectional energy transfer associated with efficient energy funneling. In this work we show that the nuclear dynamics on different excited state surfaces are responsable for an ulftrafast transient localization (i.e., self-trapping) of the electronic transition density leading to an effective energy transfer to the ethynelene-perylene trap.

RESULTS AND DISCUSSION

The room temperature experimental and calculated absorption spectra of **2** are shown in Figure 1b,c, respectively. Measured and simulated spectra have similar three-band structure with an overall red-shift of ∼30 nm observed in the calculations. The experimental bands in the 400−500 nm region are attributed to the $S_1 \leftarrow S_0$ excitation of the EPer part. This is the only peak in the spectrum featuring pronounced vibronic structure, which was not accounted for in our modeling. The experimental

DOI: 10.1021/jacs.5b04075
J. Am. Chem. Soc. 2015, 137, 11637−11644

absorption band at 375 nm, corresponding to backbone absorption, parallels the simulated band at 400 nm, which includes transitions to singlet excited states S_2−S_6. The S_2, S_3, and the sum of S_4, S_5 and S_6 states contributes 56%, 31%, and 13% to this absorption band, respectively. At higher energies, we observe an additional broad band, centered at 300 nm (the simulated spectrum peaks near 330 nm), with contributions from S_7 and higher states. The strongest contribution to this band corresponds to excitation from the ground state into S_{12}.

Figure 1d shows the ultrafast, room temperature emission of **2** detected at two different wavelengths, following excitation at 315 nm. The steady-state fluorescence spectrum of model compound **1** (dendritic backbone without the EPer sink) displays a maximum at 400 nm,[56] hence emission detected at this wavelength (purple curve) in **2** probes the transient population of the lowest energy state for the dendritic backbone **1**. The data show an initial fast rise time (300 ± 20 fs) followed by a decay (350 ± 40 fs). The initial evolution of the emission indicates dynamics in the excited state that occur at energies higher than the detection region. The 300 fs rise time encompasses all the processes occurring before the population reaches the lowest energy state of the backbone (S_2 and higher), while the decay is attributed to energy transfer from the backbone to the EPer sink. The green curve data show emission from the S_1 state located in the Eper unit and detected at 485 nm. It presents a rise time of 350 ± 20 fs, concomitant to the decay from the $S_{\geq 2}$.

Nonadiabatic excited state molecular dynamics (NAESMD) simulations model time-resolved experimental probes by exciting an ensemble of 1000 trajectories of dendrimer **2** (Figure 1a, right), which further undergo quantum transitions within the manifold of excited states. For excitation at 400 nm, the first 10 singlet excited states are included in the simulations yielding an initial state distribution with 10% in S_2, 50% in S_3, 40% in S_4/S_5 and negligible contribution from S_1. States higher than S_6 are not populated by the excitation at 400 nm (for detailed oscillator strength information, see Table S1, Supporting Information, SI).

Figure 1e shows the calculated time evolution of the populations of states from S_1 to S_6. The populations of S_3 and higher states decrease rapidly, while the population of S_2 (purple curve) rises and decays. The S_1 state population (green) increases throughout the simulation reaching a final value of ∼100% after 500 fs. Overall, an efficient ultrafast electronic energy relaxation from the initially excited high-energy states (S_n, $n \geq 3$) to the lowest S_1 excited state takes place in <500 fs, involving a transient population trap at the S_2 state. These computational results are in excellent agreement with the experimental data showed in Figure 1d.

When the simulation starts with excitations at higher energy (320 nm), many states are populated (Figure 2a); after the population reaches S_3 from all higher states, the S_3 to S_2 step becomes the bottleneck process. Following a short induction time, the population of S_2 rises and decays with a concomitant increase in the population of S_1. Figure 2b shows the tally of the populations after the high n states decayed to S_3. This figure displays a strong resemblance with the calculation following excitation at 400 nm (Figure 1e) and supports the agreement with the experimental data. In essence, all the high-energy states decay to S_3 before the population of S_2 starts to increase. As higher states are initially excited (Figure 2c), the rise time of S_2 becomes slower, but its decay remains the same, indicating that

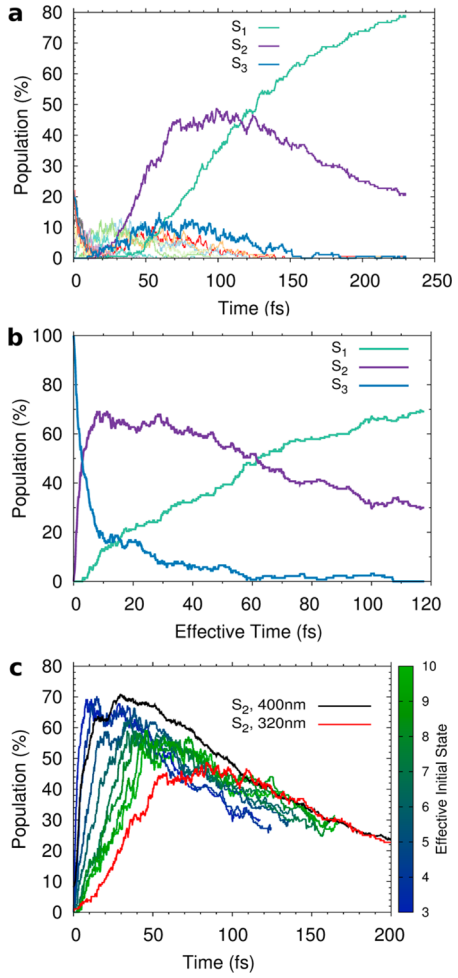

Figure 2. Populations calculated from the number of trajectories in each state at a given time. (a) The states reached by excitation at 320 nm with initial population higher than 5%. (b) The same populations but starting to count after the high n states decayed to S_3, illustrating the similarity of these results to those obtained upon 400 nm excitation (Figure 1e). (c) The population of S_2 following excitation at different wavelengths leading to initial excited states between S_3 and S_{10} (time axis uses the effective time). Highlighted in red and black are the trajectories following excitation at 400 and 320 nm, respectively. As the initial excitation reaches higher S_n, the rise time of the S_2 population becomes slower, but once the populations reaches S_2, the decay is always the same, implying a bottleneck mechanism.

irrespective of the initial excitation, all dynamics goes through a $S_3 \rightarrow S_2 \rightarrow S_1$ sequence, consistent with the experimental data.

Our computational results, validated against the experiments, provide detailed description of the excited-state dynamics and evolution of the photoexcited wave function. In order to identify universal properties of the energy-transfer events we focus on the moments before and after each state-to-state transition. To this purpose, we shift the time scale of individual trajectories, labeling as zero-delay the moment of the nonadiabatic transfer in each particular trajectory. For the discussion that follows, we refer to the "moment of the nonadiabatic transfer" as the time of effective transition or hop in which the nuclear motion change from the current state S_n to S_{n-1} and no back-hopping occurs during the rest of the trajectory.

Figure 3a shows a histogram of the potential energy difference between S_3 and S_2 states ($\Delta E_{S_3-S_2}$) as a function of

DOI: 10.1021/jacs.5b04075
J. Am. Chem. Soc. 2015, 137, 11637−11644

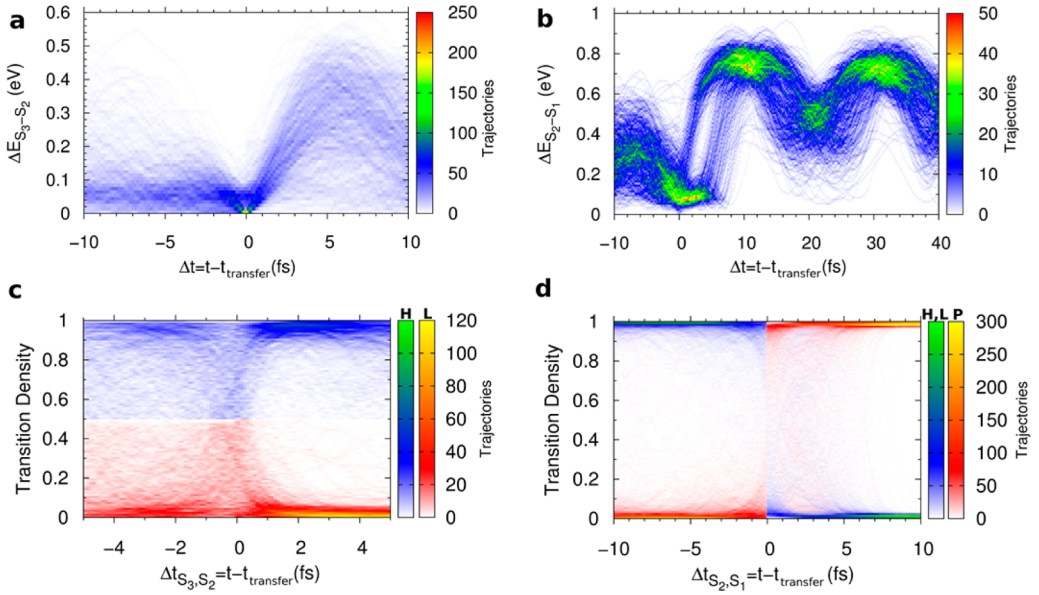

Figure 3. (a) Histogram of the difference in potential energy between two states, as a function of delay time relative to the moment of nonadiabatic transition ($S_n \rightarrow S_{n-1}$). Panel **a** shows the time around the $S_3 \rightarrow S_2$ hop. (b) Similar data for $S_2 \rightarrow S_1$ transition. The color bar corresponds to the number of trajectories at each delay time. ΔE starts high and lowers to almost 0 at the moment of transition ($\Delta t = 0$). After the hop, the two surface separate with ΔE becoming much larger, thus avoiding back transfer. The oscillatory behavior observed at longer delays corresponds to the nuclear dynamics causing the nonadiabatic coupling. Bottom two panels contain contour plots of the transition density composition before and after the hop. (c) TD around the $S_3 \rightarrow S_2$ transition. The blue-green color scale shows the TD corresponding to the moiety with higher TD (H-monodendron), and the red-yellow color scale shows the TD contours for the other moiety (L-monodendron). Before $\Delta t = 0$, the TD contour shows delocalization on the whole backbone, while after the hop, the TD contour distribution collapses onto a single monodendron. (d) TD around the $S_2 \rightarrow S_1$ transition. It shows a localized TD on the backbone as it transfers to S_1, which is fully localized on the perylene.

delay time, relative to the moment of nonadiabatic transition $S_3 \rightarrow S_2$. Before this transition, the two potential energy surfaces are separated by about 0.12 eV. At the moment of the nonadiabatic transition ($\Delta t = 0$), $\Delta E_{S_3-S_2}$ is 0.04 eV (on average), indicating the proximity to a conical intersection seam. Once the electronic population is transferred to S_2, the energy difference rapidly increases to ~0.29 eV where it becomes oscillatory due to coupled molecular motions. The increase in the energy gap after the hop prevents back uphill transitions.[57,58] This simple effect rationalizes the unidirectional energy transfer observed in these molecules.

The evolution of the difference in potential energies is similar for the $S_2 \rightarrow S_1$ transition (Figure 3b): Before the transfer to S_1, $\Delta E_{S_2-S_1}$ is 0.29 eV, becoming nearly zero at the moment of the jump and increasing to 0.73 eV about 10 fs after the transition. The oscillating behavior of ΔE observed after the electronic transfer reflects vibrational dynamics on the S_1 surface. With a period of roughly 16 fs (2084 cm^{-1}), this motion can be associated with the triple bond stretching, which was previously shown as the source of nonadiabatic coupling in phenylene-ethynylene units[59] and is shown in Figure S1, SI.

In order to analyze the intramolecular electronic energy redistribution, taking place during the electronic energy transfer, we evaluate the fraction of transition density (TD) localized on different moieties of compound **2** (eq 1, SI). The three moieties considered are the two individual monodendrons (defined by the backbone structure connected to the center phenylene unit) and the EPer (sink). At each time step we label as H-monodendron the one with higher contribution to the TD and L-monodendron the one with lower contribution to the TD.

Over 90% of trajectories that show an $S_3 \rightarrow S_2$ transition have the electronic energy located in the backbone with negligible contribution from the sink. To determine the electronic energy redistribution between monodendrons, a TD histogram was computed at every time step in the interval -5 fs $\leq \Delta t \leq 5$ fs (centered at the transfer time). Figure 3c shows the TD histogram contour plots for both monodendrons (H-monodendron in blue, L-monodendron in red) near the time of hop from S_3 to S_2. When the system is in the S_3 state, the TD is clearly delocalized over both monodendrons with the contour plots covering all values of TD between 0 and 1. This behavior changes dramatically after the transition, when the contribution of the L-monodendron fragment drops to almost 0 and most of the transition density is localized in a single monodendron (labeled H-monodendron). This fascinating result indicates that the S_3 excited state is delocalized throughout the backbone, while after the transition to S_2 it becomes localized on a single monodendron, through coupling with the nuclear dynamics.

A similar finding is observed experimentally. Transient absorption measurements on the dendrimer backbone compound **1** were performed in solution (300 K) and are presented in Figure 4a. Upon excitation at 315 nm, a negative signal appears in the transient absorption spectrum (light blue) between 305 and 420 nm. The ground-state bleach governs the signal between 305 and 385 nm, while for $\lambda > 400$ nm, stimulated emission also contributes to this negative signal (thus the relatively flatness around 400 nm). At longer wavelengths, a new, strong excited-state absorption band appears, although contribution from stimulated emission beyond 420 nm is also expected. The observed large positive signal implies that the cross section for excited-state absorption is much larger than that for stimulated emission.

DOI: 10.1021/jacs.5b04075
J. Am. Chem. Soc. 2015, 137, 11637−11644

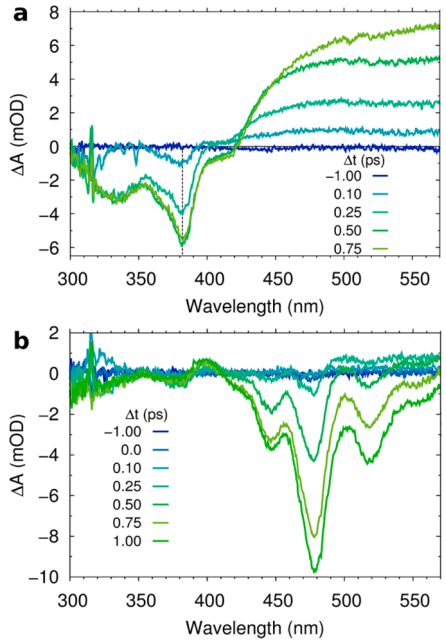

Figure 4. Transient absorption spectra of **1** (backbone) and **2** (backbone and sink). (a) Excitation localization in the backbone dendrimer. Room temperature transient absorption spectra of model compound **1** at different time delays following excitation at 315 nm. A dashed line was added to indicate the position of the band associated with the localized transition. The broadband signal rises within 250 fs, while the transient band at 382 nm continues rising, reaching a maximum at ∼500 fs. This band correlates with the red-edge peak observed in the low-temperature excitation spectrum (Figure S2, Supporting Information). (b) Energy transfer in the dendrimer with a sink. Transient absorption spectra of compound **2** showing the ultrafast energy transfer from the backbone to the EPer sink. Steady-state absorption for **2** is shown in Figure 1b. Within 300 fs, the stimulated emission signal arising from population on the Eper sink (S_1 state) is observed at $\lambda \geq 470$ nm together with the bleach from the ground state of the EPer ($425 \leq \lambda \leq 460$ nm).

The transient data show two interesting features indicative of the transfer to a more localized state. The peak of the negative signal has a maximum at 382 nm. Although the broadband bleach rises within the first 250 fs, the peak at 382 nm continues to increase in amplitude, reaching a maximum at ∼500 fs. Simultaneously with this sharp transition, the excited-state absorption on the low-energy region raises (∼750 fs) indicating a new state being populated. After that, the spectrum remains constant albeit a small 6 ps vibrational cooling component.[27,56,60,61] The "instantaneous" (within the IRF) broad bleach signal extended over the whole absorption spectrum reveals the delocalization of excitation energy on the initially excited state. The transition at 382 nm shows more localized characteristics compared to the broad bleach signal in the blue region.

To better understand the nature of the 382 nm band, we collected steady-state excitation at low temperature. While at room temperature (Figure 1b, purple), the steady-state absorption corresponds to an ensemble of transitions, from a shallow ground-state surface; at lower temperatures, the distribution of structures narrows, leading to sharper and more distinguishable bands. At 77 K, the excitation spectrum shows that absorption to the lowest energy state of the backbone gives rise to a sharp band, centered at 382 nm (Figure S2). Taken together, the experimental data provide evidence supporting the delocalization of the initially excited state, turning into a lower energy state that is more localized. Again, this is in excellent agreement with the results obtained from the NAESMD simulations. Figure 4b shows the room temperature transient absorption spectra of compound **2**, where the energy-transfer process can be clearly observed. At high energies, the bleach signal from the backbone is barely observed, whereas the bleach and stimulated emission from the sink (EPer) appears within 300 fs.

The TD calculations also provide information on the backbone-to-trap energy transfer (S_2 to S_1). Figure 3d, shows the transition density contour plots plotted for the combined monodendrons and the EPer sink. At the time of the nonadiabatic transition, the TD goes from being localized in the dendritic backbone (blue) to being localized in the perylene trap (red), where it will stay until the molecule fluoresces in a ns time scale.[29]

Spatial localization of the excitations can be better characterized using the participation number, $\mathcal{P}_{S_\alpha}$, interpreted as the number of atoms contributing to the TD for a particular state (eq 2, SI). Figure 5 shows the histogram of the $\mathcal{P}_{S_\alpha}$ for the

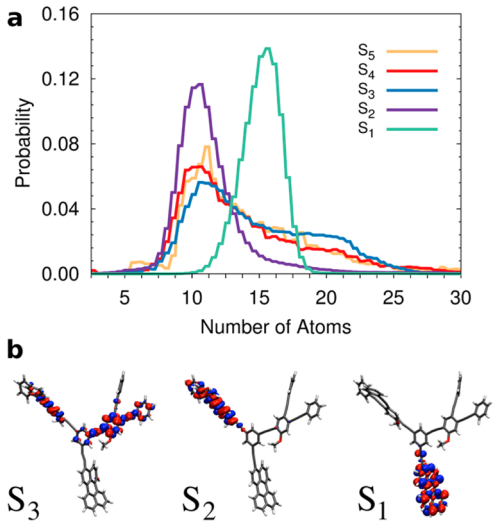

Figure 5. Contributions to the transition density of each state. (a) Histogram of the number of atoms that contribute to the first five excited states for all trajectories and times. (b) Snapshot of the orbital representation of typical transition density matrix for one trajectory; $S_{\geq 3}$ states are located over both monodendron fragments, the S_2 state is localized in one monodendron fragment, and S_1 is localized over the perylene fragment.

first five excited states and representative isocontour depictions of the TD for S_3, S_2, and S_1 states. S_3, S_4, and S_5 show broad distributions with a large number of atoms contributing to the TD, showing the delocalization over both monodendrons. Strikingly different is the S_2 histogram with a narrow distribution localized on a smaller number of atoms corresponding to one monodendron, and S_1, which is also narrow and localized in the perylene trap. A movie of a single trajectory is presented as SI highlighting these effects.

Characterization of the time evolution of the system results from fits to an $A \xrightarrow{k_1} B \xrightarrow{k_2} C$ kinetic model, where A is the initially excited state (s), B corresponds to the intermediate backbone state, and C is the final EPer sink. Upon excitation at 315 nm, the experimental results yield an initial transfer step

DOI: 10.1021/jacs.5b04075
J. Am. Chem. Soc. 2015, 137, 11637−11644

with k_1^{-1} = 300 ± 20 fs and final energy-transfer step with k_2^{-1} = 350 ± 40 fs. Upon excitation at 370 nm (Figure S3), k_2 become larger (k_2^{-1} = 250 ± 50 fs), while the initial step remains unchanged. To validate this kinetic model, we predict the rise and decay of the emission arising from the intermediate state (B) in the presence of the final sink. Figure 1d shows a remarkable agreement between the predicted (black curve) population and the observed emission (purple curve) from the intermediate state. The transient absorption of **1** and **2** (Figure 4a,b) is analyzed under the same kinetic model, and the ultrafast rise time for the ground-state bleach and excited-state absorption are obtained. From the dynamics of the molecule **1**, it takes ∼300 fs for the bleach signal to evolve into the steady-state absorption, while in **2** the energy transferred occurs within 350 fs. Interestingly, **1** data shows a spectral shift ($\tau \sim 6$ ps) associated with vibrational cooling that vanishes in **2** because the energy transfer is much faster than the vibrational relaxation. For the NAESMD computational populations, upon excitation at low energies, the kinetic model yields k_1^{-1} = 17 fs and k_2^{-1} = 100 fs. The simulations yield k_1^{-1} values somewhat sensitive to excitation wavelength, something missing in the experimental results (Figure S3). Comparison of the absorption spectra in Figure 1b,c shows that the simulated spectrum is red-shifted with respect to the experiment. The simulations show that excitations with shorter λ_{exc} populate $S_{\geq 8}$ leading to longer, less excitation-wavelength sensitive values of k_1 (∼80 fs^{-1}), hence as the excitation energy increases, the results from the simulations converge to a wavelength-insensitive k_1^{-1}. Most likely the experimental excitation reaches more than one initial state making the process slower and insensitive to λ_{exc}. Finally, a more refined model that includes uphill $S_2 \rightarrow S_3$ transitions (Figure S4b) was also considered (Figure S4). Although k_1 becomes slightly faster (k_1^{-1} =15 fs), k_2 remains similar (130^{-1} fs^{-1}) indicating that the transfer to the perylene takes place in hundreds of fs, regardless of the model.

SUMMARY AND CONCLUSIONS

Experiments and calculations have yielded a consistent picture of the ultrafast and highly efficient energy-transfer mechanism in a dendrimer. The molecule is initially excited to states that span both monodendrons ($S_{\geq 3}$), quickly collapses to a more localized excitation in S_2, and finally reaches the EPer sink (S_1) from where fluorescence occurs. The intermediate state was detected experimentally, and its localized character understood from to the analysis of the calculations.

Dynamical localization of the wave function of a transient vibrationally hot excited state has been previously studied on π conjugated polymers.[62−71] Adiabatic vibrational relaxation of the lowest electronic excited state has been linked to the spatial localization (self-trapping) of an exciton strongly coupled to torsional and C−C nuclear motions.[68,70,72] The time-scale associated with such adiabatic process is relatively slow (ps) being defined by molecular vibrations and the flow of excess vibrational energy to the bath. Our previous measurements of the vibrational relaxation in several phenylene-ethynylene dendrimers yield a time constant of between 2 and 6 ps,[56] while vibrational relaxation of the lowest excited state in polyfluorenes due to slow torsional motions can take up to tens of picoseconds resulting in a formation of self-trapped states.[73]

In this work, simulations, strongly supported by experimental data, suggest similar localization of the excited-state wave function, but strikingly occurring on an ultrafast (hundreds of femtoseconds) time scale due to nonadiabatic transitions between excited states. For this dendrimer, the large initial delocalization is due to the high density of coupled excited states (Frenkel excitons) accessed by the initial excitation and the thermal fluctuations that yield an ensemble of structures with varying conformations. The nonadiabatic electronic transitions, driven by strong coupling to high-frequency vibrational modes, quickly leads to the appearance of a spatially localized intermediate state with concomitant conversion of excess electronic energy into nuclear motions scattered across the entire molecule. These findings are in accord with previous investigations of loss of anisotropy in dendritic structures on the femtosecond time scale which have shown that vibronic relaxation can lead to localization of the exciton in ∼100 fs time excitation.[27,56,61,63−67,74] We expect that this observed non-adiabatic dynamical phenomena will be fundamental for other π-conjugated systems where a dense manifold of excited states, strong exciton−phonon coupling, and thermal disorder are the principal contributors to the ultrafast dynamics.

METHODS

Computational Method. NAESMD combines molecular dynamics with quantum transitions (MDQT)[73,75,76] with "on the fly" analytical calculations of excited-state energies, gradients, and nonadiabatic coupling terms in the framework of the collective electron oscillator (CEO) approach[77,78] and the AM1 Hamiltonian.[79] The method has been developed to simulate photoinduced dynamics in large organic conjugated molecules involving multiple coupled electronic excited states.[57,58,78] A detailed discussion of the NAESMD implementation can be found elsewhere.[59,78,80,81]

The initial step in our simulations is collection of the conformational snapshots (a set of initial coordinates and momenta) of **2** for the subsequent NAESMD simulations. Following the procedure described in SI, 1000 different structures have been accumulated.

For each snapshot, an electronic absorption spectrum was simulated by summing up Gaussian distributions, centered at the difference in energy between S_0 and S_i (with i between 1 and 30), an amplitude equal to the oscillator strength, and a bandwidth of 10 nm.

The first step before computing the NAESMD simulations involves exciting a number of the structures to an excited state that, in the ensemble, would resemble the experimental excitation process. Two families of simulations were performed. The first one involved an excitation centered at a 400 nm for an ensemble of 1000 structures, while a second group with 150 structures were excited at 320 nm. The excitation energy width is given by the transform-limited relation of a Gaussian pulse with a fwhm of 100 fs (similar to the pulses used experimentally). This enabled us to compute a Franck−Condon window defined as $g_\alpha(r, R) = \exp(-T^2(E_{laser} - E_\alpha)^2)$. Using $g_\alpha(r, R)$, in addition to the oscillator strength of each state, the initial excited state for each structure was determined.[57,82] Having chosen the initial excited state, a NAESMD simulation (trajectory) was carried out for every structure during 500 fs at a constant temperature of 300 K following protocol described in SI. More details of the parameters employed can be found elsewhere.[78]

The standard FSSH algorithm propagates quantum electronic coefficients coherently along each trajectory, without providing any mechanism for dissipating electronic coherence. This results in an internal inconsistency characterized by a disagreement between the fraction of classical trajectories evolving on a given state and the average quantum population for that state. Because of that, a large variety of methods designed to incorporate decoherence in FSSH simulations have been developed.

In the present work we have adopt the instantaneous decoherence approach previously described and tested for building blocks of phenylene ethynylene dendrimers in our article "Nonadiabatic Excited-State Molecular Dynamics: Treatment of Electronic Decoherence".[83] Briefly, the method reset the quantum amplitude of the current state

DOI: 10.1021/jacs.5b04075
J. Am. Chem. Soc. 2015, 137, 11637−11644

to unity after every attempted hop (regardless of whether hops are allowed or forbidden). This simple method is based on the assumption that wavepackets traveling on different surfaces should immediately separate in phase space and evolve independently. Our previous studies with a variety of combined polyphenylene-ethynylene chromophore units have confirmed this feature.[36,57,58] The approach has been shown to provide qualitative improvement in the agreement between classical and quantum systems at no additional computational cost.

For every trajectory, the occupied excited state, transition density matrix, nonadiabatic coupling, and geometry were stored at every classical time step, allowing us to perform an analysis of the system as an ensemble.

Experimental Method. **1** and **2** were synthesized by the group of Z. Peng at University of Missouri-Kansas City according to the procedure listed elsewhere.[48] For the spectroscopic measurement (details in SI), solutions were prepared in dry CH_2Cl_2 without further purification. The optical density of samples used in all measurements is about 0.3, which provides a concentration below 10^{-6} M to avoid any aggregation and excimer formation. The integrity of the sample was checked before and after each set of measurements.

The laser system, fluorescence upconversion, and transient absorption setup are described in detail in Atas et al.[27] Briefly, tunable excitation pulses in the 315−370 nm spectral region are used for excitation with instrument response functions of 150 (transient absorption) and 225 fs (emission) routinely recorded during each measurement session. Emission is collected by off-axis parabolic mirrors, and the excitation volume is imaged onto a 300 μm β-Barium Borate (β-BBO) crystal where it is overlapped in space and time with a gate beam to generate a nonlinear response signal in the UV, which is dispersed and detected by a PMT. Transient absorption is probed with a broadband pulse (315−720 nm) generated in a CaF_2 plate and detected by a CCD camera. After polarization filtering, the magic angle transient absorption signal is reconstructed as a function of pump−probe delay time. Data analysis involves the convolution of decay and rise time functions with the corresponding experimental instrument response function (IRF) for each experiment.

■ ASSOCIATED CONTENT

Supporting Information

Figure S1 presents the triple bond distances as a function of time. Figure S2 shows the excitation and emission spectra of compound 1, while Figure S3 shows time-resolved emission following two different excitation wavelengths for compounds **1** and **2**. Figure S4 includes a description of hops between states in terms of which states are connected and their time-evolution. In Table S1 we present the averaged oscillator strengths for each electronic state at the wavelength used for the calculations. The kinetic modeling for experiments and calculations is shown as well as additional information on methods including information on the construction of the ensemble, the NAESMD trajectories, and experimental conditions. Finally, the definitions of the different descriptors (participation number and fraction of TD) used in the manuscript. The Supporting Information is available free of charge on the ACS Publications website at DOI: 10.1021/jacs.5b04075.

■ AUTHOR INFORMATION

Corresponding Authors

*kleiman@ufl.edu

*roitberg@ufl.edu

Present Addresses

[∥]Department of Chemistry, Universidad Nacional de Colombia, Bogotá, Colombia

[⊥]Department of Biomedical Engineering, Boston University, Boston, MA, 02215, United States

[#]AB-Schomburg Yapi Kimyasallari A. S., 34736 Kozyatağı-Kadiköy, Istanbul, Turkey

[▽]Department of Chemistry, Louisiana State University, Baton Rouge, LA, 70803, United States

Notes

The authors declare no competing financial interest.

■ ACKNOWLEDGMENTS

This work was partially supported by CONICET, UNQ, ANPCyT (Grant PICT-2010-2375), National Science Foundation Grant CHE-1058638, and U.S. Department of Energy and Los Alamos LDRD funds. We acknowledge the University of Florida Research Computing for providing computational resources and support that have contributed to the research results reported in this publication, and the computer time allocated through NSF XSEDE MCA01S027. We also acknowledge Z. Peng at University of Missouri-Kansas City for providing us with the samples used in these experiments.

■ REFERENCES

(1) Balzani, V.; Credi, A.; Venturi, M. *ChemSusChem* **2008**, *1*, 26−58.
(2) Holdren, J. P. *Science* **2007**, *315*, 737.
(3) Scholes, G. D.; Fleming, G. R.; Olaya-Castro, A.; van Grondelle, R. *Nat. Chem.* **2011**, *3*, 763−774.
(4) Frischmann, P. D.; Mahata, K.; Würthner, F. *Chem. Soc. Rev.* **2013**, *42*, 1847−1870.
(5) Mathew, S.; Yella, A.; Gao, P.; Humphry-Baker, R.; Curchod, B. F. E.; Ashari-Astani, N.; Tavernelli, I.; Rothlisberger, U.; Nazeeruddin, M. K.; Grätzel, M. *Nat. Chem.* **2014**, *6*, 242−247.
(6) Halpin, A.; Johnson, P. J. M.; Tempelaar, R.; Murphy, R. S.; Knoester, J.; Jansen, T. L. C.; Miller, R. J. D. *Nat. Chem.* **2014**, *6*, 196−201.
(7) Engel, G. S.; Calhoun, T. R.; Read, E. L.; Ahn, T.-K.; Mančal, T.; Cheng, Y.-C.; Blankenship, R. E.; Fleming, G. R. *Nature* **2007**, *446*, 782−786.
(8) Andrews, D. L. *J. Mater. Res.* **2012**, *27*, 627−638.
(9) Adronov, A.; Fréchet, J. *Chem. Commun.* **2000**, *18*, 1701−1710.
(10) Nelson, D. L.; Lehninger, A. L.; Cox, M. M. *Lehninger Principles of Biochemistry*; W. H. Freeman: New York, 2008.
(11) Hu, X.; Damjanović, A.; Ritz, T.; Schulten, K. *Proc. Natl. Acad. Sci. U. S. A.* **1998**, *95*, 5935−5941.
(12) Caycedo-Soler, F.; Rodriguez, F. J.; Quiroga, L.; Johnson, N. F. *Phys. Rev. Lett.* **2010**, *104*, 158302.
(13) Ishida, Y.; Shimada, T.; Masui, D.; Tachibana, H.; Inoue, H.; Takagi, S. *J. Am. Chem. Soc.* **2011**, *133*, 14280−14286.
(14) Lefler, K. M.; Kim, C. H.; Wu, Y.-L.; Wasielewski, M. R. *J. Phys. Chem. Lett.* **2014**, *5*, 1608−1615.
(15) Lee, C. Y.; Farha, O. K.; Hong, B. J.; Sarjeant, A. A.; Nguyen, S. T.; Hupp, J. T. *J. Am. Chem. Soc.* **2011**, *133*, 15858−15861.
(16) Chen, L.; Honsho, Y.; Seki, S.; Jiang, D. *J. Am. Chem. Soc.* **2010**, *132*, 6742−6748.
(17) Gilat, S. L.; Adronov, A.; Fréchet, J. M. J. *Angew. Chem., Int. Ed.* **1999**, *38*, 1422−1427.
(18) Adronov, A.; Robello, D. R.; Fréchet, J. M. J. *J. Polym. Sci., Part A: Polym. Chem.* **2001**, *39*, 1366−1373.
(19) Kozaki, M.; Suzuki, S.; Okada, K. *Chem. Lett.* **2013**, *42*, 1112−1118.
(20) Inoue, K. *Prog. Polym. Sci.* **2000**, *25*, 453−571.
(21) Devadoss, C.; Bharathi, P.; Moore, J. S. *J. Am. Chem. Soc.* **1996**, *118*, 9635−9644.
(22) Oesterling, I.; Müllen, K. *J. Am. Chem. Soc.* **2007**, *129*, 4595−4605.
(23) Ziessel, R.; Harriman, A. *Chem. Commun.* **2011**, *47*, 611−631.
(24) Xu, Z.; Kahr, M.; Walker, K. L.; Wilkins, C. L.; Moore, J. S. *J. Am. Chem. Soc.* **1994**, *116*, 4537−4550.
(25) Li, W.-S.; Aida, T. *Chem. Rev.* **2009**, *109*, 6047−6076.
(26) Lo, S.-C.; Burn, P. L. *Chem. Rev.* **2007**, *107*, 1097−1116.

DOI: 10.1021/jacs.5b04075
J. Am. Chem. Soc. 2015, 137, 11637−11644

(27) Atas, E.; Peng, Z.; Kleiman, V. D. *J. Phys. Chem. B* **2005**, *109*, 13553−13560.
(28) Melinger, J. S.; Pan, Y.; Kleiman, V. D.; Peng, Z.; Davis, B. L.; McMorrow, D.; Lu, M. *J. Am. Chem. Soc.* **2002**, *124*, 12002−12012.
(29) Peng, Z.; Melinger, J. S.; Kleiman, V. *Photosynth. Res.* **2006**, *87*, 115−131.
(30) Moore, J. S.; Xu, Z. *Macromolecules* **1991**, *24*, 5893−5894.
(31) Morgenroth, F.; Reuther, E.; Müllen, K. *Angew. Chem., Int. Ed. Engl.* **1997**, *36*, 631−634.
(32) Aida, T.; Jiang, D.-L.; Yashima, E.; Okamoto, Y. *Thin Solid Films* **1998**, *331*, 254−258.
(33) Wu, C.; Malinin, S. V.; Tretiak, S.; Chernyak, V. Y. *Nat. Phys.* **2006**, *2*, 631−635.
(34) Aggarwal, A. V.; Thiessen, A.; Idelson, A.; Kalle, D.; Würsch, D.; Stangl, T.; Steiner, F.; Jester, S.-S.; Vogelsang, J.; Höger, S.; Lupton, J. M. *Nat. Chem.* **2013**, *5*, 964−970.
(35) Kleiman, V. D.; Melinger, J. S.; McMorrow, D. *J. Phys. Chem. B* **2001**, *105*, 5595−5598.
(36) Fernandez-Alberti, S.; Kleiman, V. D.; Tretiak, S.; Roitberg, A. E. *J. Phys. Chem. Lett.* **2010**, *1*, 2699−2704.
(37) Swallen, S. F.; Kopelman, R.; Moore, J. S.; Devadoss, C. *J. Mol. Struct.* **1999**, *485*−*486*, 585−597.
(38) Rana, D.; Gangopadhyay, G. *Chem. Phys. Lett.* **2001**, *334*, 314−324.
(39) Barford, W.; Boczarow, I.; Wharram, T. *J. Phys. Chem. A* **2011**, *115*, 9111−9119.
(40) Vögtle, F.; Gorka, M.; Hesse, R.; Ceroni, P.; Maestri, M.; Balzani, V. *Photochem. Photobiol. Sci.* **2002**, *1*, 45−51.
(41) Frechet, J. M. *Science* **1994**, *263*, 1710−1715.
(42) Xu, Z.; Moore, J. S. *Acta Polym.* **1994**, *45*, 83−87.
(43) Shortreed, M. R.; Swallen, S. F.; Shi, Z.-Y.; Tan, W.; Xu, Z.; Devadoss, C.; Moore, J. S.; Kopelman, R. *J. Phys. Chem. B* **1997**, *101*, 6318−6322.
(44) Ortiz, W.; Krueger, B. P.; Kleiman, V. D.; Krause, J. L.; Roitberg, A. E. *J. Phys. Chem. B* **2005**, *109*, 11512−11519.
(45) Palma, J. L.; Atas, E.; Hardison, L.; Marder, T. B.; Collings, J. C.; Beeby, A.; Melinger, J. S.; Krause, J. L.; Kleiman, V. D.; Roitberg, A. E. *J. Phys. Chem. C* **2010**, *114*, 20702−20712.
(46) Kuroda, D. G.; Singh, C. P.; Peng, Z.; Kleiman, V. D. *Science* **2009**, *326*, 263−267.
(47) Atas, E.; Mair, C.; Melinger, J. S.; Peng, Z.; Kleiman, V. D. In *Ultrafast Phenomena XIV*; Kobayashi, P. T., Okada, P. T., Kobayashi, P. T., Nelson, P. K. A., Silvestri, P. S. D., Eds.; Springer Series in Chemical Physics; Springer: Berlin Heidelberg, 2005; pp 456−458.
(48) Pan, Y.; Lu, M.; Peng, Z.; Melinger, J. S. *J. Org. Chem.* **2003**, *68*, 6952−6958.
(49) Duvanel, G.; Grilj, J.; Schuwey, A.; Gossauer, A.; Vauthey, E. *Photochem. Photobiol. Sci. Off. J. Eur. Photochem. Assoc. Eur. Soc. Photobiol.* **2007**, *6*, 956−963.
(50) Beenken, W. J. D.; Dahlbom, M.; Kjellberg, P.; Pullerits, T. *J. Chem. Phys.* **2002**, *117*, 5810−5820.
(51) Tiwari, V.; Peters, W. K.; Jonas, D. M. *Proc. Natl. Acad. Sci. U. S. A.* **2013**, *110*, 1203−1208.
(52) Christensson, N.; Kauffmann, H. F.; Pullerits, T.; Mančal, T. *J. Phys. Chem. B* **2012**, *116*, 7449−7454.
(53) Kopelman, R.; Shortreed, M.; Shi, Z.-Y.; Tan, W.; Xu, Z.; Moore, J. S.; Bar-Haim, A.; Klafter, J. *Phys. Rev. Lett.* **1997**, *78*, 1239−1242.
(54) Swallen, S. F.; Shi, Z.-Y.; Tan, W.; Xu, Z.; Moore, J. S.; Kopelman, R. *J. Lumin.* **1998**, *76*−*77*, 193−196.
(55) Pouthier, V. *J. Chem. Phys.* **2013**, *139*, 234111.
(56) Atas, E. Ultrafast time resolved excitation dynamics in conjugated dendrimers. *Ph.D. Thesis*, University of Florida, Gainesville, FL, 2006.
(57) Fernandez-Alberti, S.; Roitberg, A. E.; Kleiman, V. D.; Nelson, T.; Tretiak, S. *J. Chem. Phys.* **2012**, *137*, 22A526.
(58) Fernandez-Alberti, S.; Kleiman, V. D.; Tretiak, S.; Roitberg, A. E. *J. Phys. Chem. A* **2009**, *113*, 7535−7542.
(59) Galindo, J. F.; Fernandez-Alberti, S.; Roitberg, A. E. *J. Phys. Chem. C* **2013**, *117*, 26517−26528.
(60) Karni, Y.; Jordens, S.; De Belder, G.; Schweitzer, G.; Hofkens, J.; Gensch, T.; Maus, M.; De Schryver, F. C.; Hermann, A.; Müllen, K. *Chem. Phys. Lett.* **1999**, *310*, 73−78.
(61) De Belder, G.; Jordens, S.; Lor, M.; Schweitzer, G.; De, R.; Weil, T.; Herrmann, A.; Wiesler, U. K.; Müllen, K.; De Schryver, F. C. *J. Photochem. Photobiol., A* **2001**, *145*, 61−70.
(62) Stafström, S. *Chem. Soc. Rev.* **2010**, *39*, 2484−2499.
(63) Ruseckas, A.; Wood, P.; Samuel, I. D. W.; Webster, G. R.; Mitchell, W. J.; Burn, P. L.; Sundström, V. *Phys. Rev. B: Condens. Matter Mater. Phys.* **2005**, *72*, 115214.
(64) Montgomery, N. A.; Hedley, G. J.; Ruseckas, A.; Denis, J. C.; Schumacher, S.; Kanibolotsky, A. L.; Skabara, P. J.; Galbraith, I.; Turnbull, G. A.; Samuel, I. D. W. *Phys. Chem. Chem. Phys.* **2012**, *14*, 9176−9184.
(65) Ruseckas, A.; Samuel, I. D. W. *Phys. Status Solidi C* **2006**, *3*, 263−266.
(66) Montgomery, N. A.; Denis, J. C.; Schumacher, S.; Ruseckas, A.; Skabara, P. J.; Kanibolotsky, A.; Paterson, M. J.; Galbraith, I.; Turnbull, G. A.; Samuel, I. D. W. *J. Phys. Chem. A* **2011**, *115*, 2913−2919.
(67) Ranasinghe, M. I.; Hager, M. W.; Gorman, C. B.; Goodson, T. *J. Phys. Chem. B* **2004**, *108*, 8543−8549.
(68) Beenken, W. J. D.; Pullerits, T. *J. Phys. Chem. B* **2004**, *108*, 6164−6169.
(69) Hennebicq, E.; Pourtois, G.; Scholes, G. D.; Herz, L. M.; Russell, D. M.; Silva, C.; Setayesh, S.; Grimsdale, A. C.; Müllen, K.; Brédas, J.-L.; Beljonne, D. *J. Am. Chem. Soc.* **2005**, *127*, 4744−4762.
(70) Tretiak, S.; Saxena, A.; Martin, R. L.; Bishop, A. R. *Phys. Rev. Lett.* **2002**, *89*, 097402.
(71) Nakano, M.; Kishi, R.; Minami, T.; Yoneda, K. *Molecules* **2009**, *14*, 3700−3718.
(72) Karabunarliev, S.; Bittner, E. R. *J. Chem. Phys.* **2003**, *118*, 4291−4296.
(73) Clark, J.; Nelson, T.; Tretiak, S.; Cirmi, G.; Lanzani, G. *Nat. Phys.* **2012**, *8*, 225−231.
(74) Komurlu, S. Photophysics and Energy Transfer of Novel Conjugated Metarials by Ultrafast Spectroscopy. *Ph.D. Thesis*, University of Florida, Gainesville, FL, 2012.
(75) Tully, J. C. *J. Chem. Phys.* **1990**, *93*, 1061−1071.
(76) Tully, J. C. *J. Chem. Phys.* **2012**, *137*, 22A301.
(77) Tretiak, S.; Mukamel, S. *Chem. Rev.* **2002**, *102*, 3171−3212.
(78) Nelson, T.; Fernandez-Alberti, S.; Chernyak, V.; Roitberg, A. E.; Tretiak, S. *J. Phys. Chem. B* **2011**, *115*, 5402−5414.
(79) Dewar, M. J. S.; Zoebisch, E. G.; Healy, E. F.; Stewart, J. J. P. *J. Am. Chem. Soc.* **1985**, *107*, 3902−3909.
(80) Nelson, T.; Fernandez-Alberti, S.; Roitberg, A. E.; Tretiak, S. *Acc. Chem. Res.* **2014**, *47*, 1155−1164.
(81) Nelson, T. Nonadiabatic excited state molecular dynamics: perspectives for a robust future. *Ph.D. Thesis*, University of Rochester, Rochester, NY, 2013.
(82) Fernandez-Alberti, S.; Roitberg, A. E.; Nelson, T.; Tretiak, S. *J. Chem. Phys.* **2012**, *137*, 014512.
(83) Nelson, T.; Fernandez-Alberti, S.; Roitberg, A. E.; Tretiak, S. *J. Chem. Phys.* **2013**, *138*, 224111.
(84) Joblin, C.; Salama, F.; Allamandola, L. *J. Chem. Phys.* **1999**, *110*, 7287−7297.

DOI: 10.1021/jacs.5b04075
J. Am. Chem. Soc. 2015, 137, 11637−11644